Cell Motility and the Cytoskeleton 60:104–120 (2005)

Actin and Alpha-Actinin Dynamics in the Adhesion and Motility of EPEC and EHEC on Host Cells

Nathan C. Shaner, Joseph W. Sanger, and Jean M. Sanger*

Department of Cell and Developmental Biology, University of Pennsylvania School of Medicine, Philadelphia, Pennsylvania

Two pathogenic *Escherichia coli*, Enteropathogenic *E. coli* (EPEC) and Enterohemorrhagic *E. coli* (EHEC), adhere to the outside of host cells and induce cytoskeletal rearrangements leading to the formation of membrane-encased pedestals comprised of actin filaments and other associated proteins beneath the bacteria. The structure of the pedestals induced by the two pathogens appears similar, although those induced by EHEC are shorter in length. Fluorescence Recovery After Photobleaching (FRAP) was used to determine potential differences of actin polymerization in EPEC and EHEC induced pedestals in cultured PtK2 cells expressing either Green or Yellow Fluorescent Protein (GFP or YFP) fused to actin or alpha-actinin. When all the fluorescent actin in a pedestal on EPEC-infected cells was photobleached, fluorescence recovery first occurred directly beneath the bacterium in a band that grew wider at a rate of one micron/minute. Consistently observed in all EPEC-induced pedestals, whether they were stationary, lengthening, or translocating, the rate of actin polymerization that occurred at the pedestal tip was approximately 1 μm/min. Overall, a much slower rate of actin polymerization was measured in long EHEC-induced pedestals. In contrast to the dynamics of GFP-actin, recovery of GFP-alpha-actinin fluorescence was not polarized, with the actin cross-linking protein exchanging all the length of the EPEC/EHEC induced pedestals. Surprisingly, the depolymerization and retrograde flow of pedestal actin, as well as pedestal translocations, were inhibited reversibly by either 2,3-butanedione monoxime (BDM) or by a combination of sodium azide and 2-deoxy D-glucose, leading to an increase in the lengths of the pedestals. A simple physical model was developed to describe elongation and translocation of EPEC/EHEC pedestals in terms of actin polymerization and depolymerization dynamics. Cell Motil. Cytoskeleton 60:104–120, 2005.

Key words: actin; alpha-actinin; EPEC; EHEC; FRAP; pathogens

Abbreviations: BDM: 2,3-butanedione monoxime; EPEC: Enteropathogenic *E. coli*; EHEC: Enterohemorrhagic *E. coli*; FRAP: fluorescence recovery after photobleaching; GFP: green fluorescent protein; YFP: yellow fluorescent protein.

Contract grant sponsor: United States Department of Agriculture.

*Correspondence to: Dr. Jean M. Sanger, Department of Cell and Developmental Biology, University of Pennsylvania School of Medicine, 421 Curie Boulevard, Philadelphia, PA 19104-6058.
E-mail: sangerjm@mail.med.upenn.edu

Received 11 June 2004; accepted 15 October 2004

Published online in Wiley InterScience (www.interscience.wiley.com).
DOI: 10.1002/cm.20047

INTRODUCTION

There are a number of bacteria whose interactions with host cells subvert the cells' actin machinery to generate movement of the bacteria [Frischnecht and Way, 2001]. One group of these bacteria (*Listeria, Shigella, Rickettsia*) enters host cells where bacterial surface proteins interact with host proteins to mediate actin polymerization resulting in a tail-like column of actin filaments and concurrent intrahost movement of the bacteria [Cossart and Sansonetti, 2004]. A second group of bacteria including Enteropathogenic *Escherichia coli* (EPEC), Enterohemorrhagic *E. coli* (EHEC; *E. coli* O157:H7), strains of *Hafnia alvei, Citrobacter freundii* biotype 4280 and *Helicobacter pylori,* adhere to target cells and while remaining extracellular induce rearrangements of the actin cytoskeleton and cause gastrointestinal diseases [reviewed in Goosney et al., 2000a; Kaper et al., 2004]. Cytoplasmic actin accumulates beneath the attached bacteria in a column or pedestal that is diagnostic for these infections [Knutton et al., 1987; 1989]. The pedestals with the attached EPEC often extend several microns or more above the cell surface, and translocate along the surface of the host cell in a cytochalasin-D sensitive manner, suggestive that actin polymerization was responsible for the movement [Sanger et al., 1996]. Prolonged infection in epithelial cells results in the eventual loss of microvilli and alteration in calcium homeostasis [Hecht, 1999].

At the molecular level, the interaction of EPEC and EHEC with host cells occurs through bacterial adhesion to the outer surface of the host cell membrane [Knutton et al., 1989; Rosenshine et al., 1996; Goosney et al., 2000a]. This attachment is effected when the bacterial membrane protein, intimin, binds to a bacterially encoded receptor, Tir (translocated intimin receptor), that is inserted into the host cell membrane by the bacteria [Kenny et al., 1997]. The attachment of EPEC/EHEC induces the focused accumulation of actin filaments and actin-associated proteins beneath the attached bacteria [Freeman et al., 2000; Goosney et al., 2000b, 2001; Huang et al., 2002]. EPEC Tir can bind alpha-actinin and other actin-associated proteins in the pedestal [Freeman et al., 2000; Goosney, et al, 2001; Huang et al., 2002]. The Tir-associating protein cortactin is located in EPEC/EHEC pedestals, and is necessary for actin assembly in the formation of EPEC pedestals [Cantarelli et al., 2002]. In addition to actin binding proteins, Tir has also been reported to bind the intermediate filament protein, cytokeratin-18, in a yeast two-hybrid assay, and this protein also appears to be necessary for pedestal formation [Batchelor et al., 2004].

Although the pedestals induced by EPEC or EHEC appear to be similar in structure [Ismali et al., 1995; DeVinney et al., 1999; Goosney et al., 2000], they differ in their assembly properties [DeVinney et al., 1999, 2001a,b; Kenny, 1999; Goosney et al., 2001]. EPEC Tir, but not EHEC Tir, must be tyrosine phosphorylated in the host cell for pedestal formation [DeVinney et al., 2001a, b]. In a comparative analysis of 25 eukaryotic proteins associated with EPEC and EHEC pedestals, Goosney et al. [2001] and Gruenheid et al. [2001] found only three mammalian components to be absent in EHEC pedestals, the adapter proteins Grb2 CrkII, and Nck [Campellone et al., 2002]. Grb2 and CrkII are composed of two SH3 domains and one SH2 domain, enabling them to bind a number of signaling and cytoskeletal proteins [Goosney et al., 2001; Carlier et al., 2000]. Grb2 has been found to enhance the binding of N-WASP (Neural Wiskott-Aldrich syndrome protein) with the ARP2/3 (actin-related protein) complex to promote actin polymerization [Carlier et al., 2000]. N-WASP, ARP2/3 complex, and cofilin are present in EPEC/EHEC pedestals [Goosney et al., 2001]. N-WASP is required for pedestal formation by both EPEC and EHEC, although the two bacteria recruit N-WASP by different mechanisms [Lommel et al., 2001, 2004].

In this study, we report that the dynamics of actin filament formation differ dramatically between EPEC and EHEC induced pedestals. Actin assembly, as analyzed by fluorescence recovery after photobleaching (FRAP) in host cells expressing Green or Yellow Fluorescent Protein (GFP/YFP), was initiated proximal to the bacteria and proceeded distally in a retrograde direction before disassembly was completed at the base of the pedestal. The rate of actin polymerization in EPEC-induced pedestals was fivefold faster than that in EHEC-induced pedestals, about 1 μm/min for EPEC versus about 0.2 μm/min for EHEC. Furthermore, the retrograde movement of newly incorporated actin and actin depolymerization in EPEC/EHEC pedestals were inhibited reversibly by sodium azide/2-deoxy D-glucose or BDM treatment. A simple model, requiring only actin polymerization, depolymerization, and the tethering of actin filaments at the interface between the pedestal and the cell body was developed to explain the elongation and translocation of EPEC/EHEC pedestals on the surfaces of infected cells.

MATERIALS AND METHODS

Tissue Culture and Bacterial Strains

Enteropathogenic *E. coli* (EPEC), strains E23348/69 (wild type strain) and JPN-15 (strain lacking the pilus gene bfpA) [Jerse et al., 1990] or Enterohemorrhagic *E. coli* (EHEC), O157:H7, strain 85-170 (strain that has spontaneously lost the genes encoding Shiga toxin, a gift from Dr. James Kaper, University of Maryland,

Baltimore, MD) were used to infect PtK2 cells, a renal epithelium line that has proved advantageous for the imaging of host cell responses to infectious bacteria [Dabiri et al., 1990; Sanger et al., 1992, 1996; Malish et al., 2003]. The PtK2 cells are grown in a medium (PtK2 medium) consisting of 100 ml of Eagle's minimum essential medium (MEM), 1 ml of 100 mM glutamine, and 10% fetal bovine serum. For infections, overnight cultures of EPEC and EHEC were grown in 2 ml LB medium in a 37°C incubator as described by Sanger et al. [1996]. One milliliter of overnight EPEC or EHEC culture was pelleted at 4,000 RPM for 2 min in a tabletop microfuge. The supernatant was discarded, and the pellet was suspended in 1 ml of PtK2 medium [Sanger et al., 1996], and then repelleted at 8,000 RPM for 2 min. The supernatant was again discarded, and the pellet suspended in 1 ml of PtK2 medium. To infect the PtK2, cells bathe in 2 ml of PtK2 medium, 5 μl of the bacterial suspension was added to the center of a 35-mm glass-bottom dish of near confluent PtK2 cells, and incubated at 37°C and 5% CO_2. Cells were checked at regular intervals for bacterial adhesion and were rinsed with fresh PtK2 medium. Immediately before imaging, the medium was replaced with pre-warmed PtK2 growth medium containing 25 mM HEPES buffer, pH 7.0.

Transfection of Cells

PtK2 cells were grown on 35-mm glass-bottom dishes (MatTek, Ashland, MA) as described by Ayoob et al. [2000b]. The plasmid pEYFP-actin was created by inserting the cDNA for human cytoplasmic-beta-actin (Clontech, Palo Alto, CA) into the pEYFP-C1 vector (Clontech). The plasmid pEYFP-alpha-actinin was created by inserting previously cloned alpha-actinin cDNA [Dabiri et al., 1997] into the pEYFP-N1 vector (Clontech). PtK2 cells were transfected with pEGFP-actin (purchased from Clontech), pEYFP-actin, pEGFP-alpha-actinin [Dabiri et al., 1999], or pEYFP-alpha-actinin following the protocol previously described [Ayoob et al., 2000a, 2001]. Briefly, 10 μl of lipofectin was combined with 200 μl Opti-MEM (Life Technologies, Inc., Rockville, MD) and incubated at room temperature for 45 min. To this solution, 1 μg of plasmid DNA in 200 μl of Opti-MEM was added, vortexed briefly, and incubated at room temperature for 15 min. After incubation, an additional 0.6 ml of Opti-MEM was added, and the well-mixed solution was overlaid onto a 35-mm glass-bottom dish of 60–80% confluent PtK2 cells from which the growth medium had been removed. The dish was incubated for 3 h in a 37°C 5% CO_2 incubator. After incubation, the dish was rinsed twice with growth medium and then returned to the incubator. Transfected cells, 2 to 4 days post-transfection, were infected by EPEC or EHEC using methods described above.

Actin Preparation, Permeabilization, and Western Blots Using Anti-Cofilin Antibodies

Rhodamine-labeled actin monomers were prepared from chicken or rabbit acetone powders as previously described [Turnacioglu et al., 1998]. Enteropathogenic *E. coli* (EPEC) was used to infect PtK2 cells [Sanger et al., 1996]. Infected cells were permeabilized according to procedures described by Symons and Mitchison [1991] and Cudmore et al. [1996]. Saponized infected cells were exposed to 0.3 μM of rhodamine-labeled monomeric actin for two different time periods, 1 and 10 min. Some saponized-infected cells were also exposed to rhodamine-labeled monomeric actin in the presence of 5 μM of cytochalasin D for 1 and 10 min. Permeabilized infected cells were then fixed for staining with fluorescence probes as previously described [Sanger et al., 1996]. Rhodamine phalloidin was obtained from Fluka (Ronkokoma, NY). Alexa 488-Phalloidin and fluorescein-labeled phalloidin were purchased from Molecular Probes (Eugene, OR). Cytochalasin-D was purchased from Sigma Corp. (St. Louis, MO), dissolved in dimethyl sulfoxide, and used at a concentration of 5 μM. Specific antibodies directed against adf/cofilin and phosphorylated cofilin were a generous gift of Dr. James R. Bamburg (Colorado State University, Fort Collins, CO) [Meberg et al., 1998]. Fluorescent images were obtained using a Nikon Diaphot 200 inverted fluorescence microscope. Photographic images were assembled using MetaMorph software (Universal Imaging Corp., West Chester, PA) and Adobe Photoshop (San Jose, CA).

Confocal Imaging and Photobleaching

Cells were observed with a Zeiss LSM 510 confocal microscope, using a 63× water-immersion objective, an excitation wavelength of 488 nm for GFP probes and 514 nm for YFP probes. A long-pass 505-nm emission filter was used for both GFP and YFP probes. The pinhole was set at 1,000 μm in order to image the entire thickness of the pedestals. Pedestals were chosen that were as close as possible to being in a single focal plane. Regions of interest were bleached using the Zeiss software, with the laser at 100% intensity. Post-bleach images were obtained periodically at time points between 5 and 20 seconds apart.

Use of Inhibitors

PtK2 cells infected with EPEC were exposed to ML-7 (Sigma, St. Louis, MO) at concentrations varying from 10 to 30 μm for 1 to 2 h to determine if inhibition of non-muscle myosin II affected either movement of the pedestal on the surfaces of the cells or the retrograde movement of the fluorescent actin bundles inside the pedestals. A combination of inhibitors (20 mM sodium azide and 10 mM 2-deoxy D-glucose) that are known to

lower the ATP concentrations of cells [Sanger et al., 1983; Glascott et al., 1987] were applied to infected cells. BDM (10 to 50 mM), a low-affinity inhibitor of skeletal muscle myosin II, was used to determine if the rearward movement of actin filaments inside pedestals was inhibited. Both groups of inhibitors were applied to cells that had previously been imaged under control conditions. The inhibitors were replaced after 30 to 60 min with control medium.

Data Analysis

Data were analyzed using MetaMorph software on a PC workstation. Short Pedestals: Stacks of images in each time series were aligned and the average fluorescence intensity of the bleached pedestal, an unbleached pedestal, and a background region were recorded for each time point. The background intensity was subtracted from the bleached and unbleached intensity values, and the ratio was calculated between the resulting corrected intensities. Finally, the data were normalized to the peak ratio of bleached/unbleached intensity. Long Pedestals: Stacks of images in each time series were aligned and the distance scale calibrated. The average speed of actin polymerization was then calculated by dividing the distance moved by a bleached band by the total time of observation.

RESULTS

Confocal Analysis of Fixed Infected Cells

EPEC- and EHEC-infected cells are characterized by specialized surface membrane projections that encase bundles of actin filaments (Fig. 1). The projections, termed pedestals [Knutton et al., 1987; 1989], form beneath adherent EPEC/EHEC and can reach lengths of up to 10 μm. In short pedestals, the actin beneath the EPEC appears as ski-like bars that, by confocal microscopy, measure 0.25 to 2 μm in the Z-axis [Sanger et al., 1996]. EHEC short pedestals are usually no more than 0.25 μm in length. Longer pedestals, i.e., 0.5 μm or more, are much easier to find in EPEC- than in EHEC-infected host cells. In live cells, pedestal length can remain constant or can be dynamic, with episodes of growth and shortening. Measurements of the fluorescence intensity of phalloidin-stained actin in the pedestals indicated that the actin concentration is highest at the apical tip and uniform behind the tip for a distance that varies between pedestals, and is followed by a gradual decrease in the fluorescence toward the distal end of the pedestal (Fig. 1).

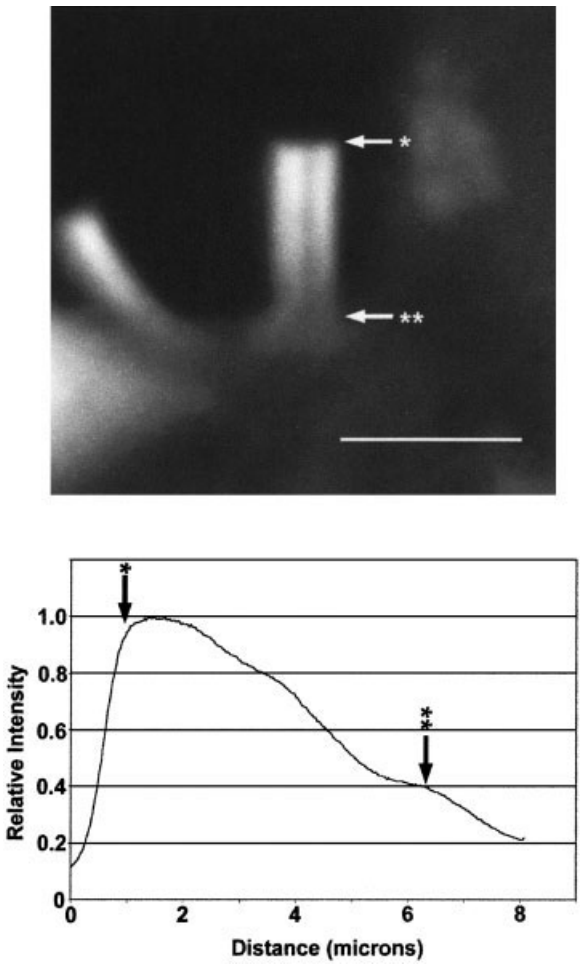

Fig. 1. EPEC-infected PtK2 cells fixed and stained with Alexa 488-Phalloidin to show the distribution of F-actin along the pedestal. Line scan along length of pedestal starting at EPEC attachment site. There is a small plateau of intensity near the externally attached EPEC (*single asterisk*) followed by a gradual loss of actin fluorescent intensity along the length of the pedestal (*double asterisks* indicate attachment of pedestal to cell body). The graph indicates that about half of the actin filaments have depolymerized 4 μm from the tip of this 5-and-a-half-micron-long pedestal. Scale bar = 5 μm.

Actin Incorporation Into Saponized Infected Cells

To determine the sites of actin polymerization in EPEC-infected cells, the cells were permeabilized with saponin and exposed to rhodamine-labeled monomer actin, at concentrations required for addition of monomers to the fast-growing or barbed ends of actin filaments (see Materials and Methods), and then fixed and stained with FITC-phalloidin. After 1-minute exposure to the monomer actin, fluorescence was detected in a band beneath the attached EPEC at the tip of the full length of the actin in the pedestals (Fig. 2A,B). When double pedestals formed, one on each side of an individual EPEC [Freeman et al., 2000], the rhodamine actin incorporation occurred just beneath both sides of the attached EPEC (Fig. 2C,D). When the saponized cells were incubated with the actin monomers for 10 min, rhodamine-labeled actin was detected along the full

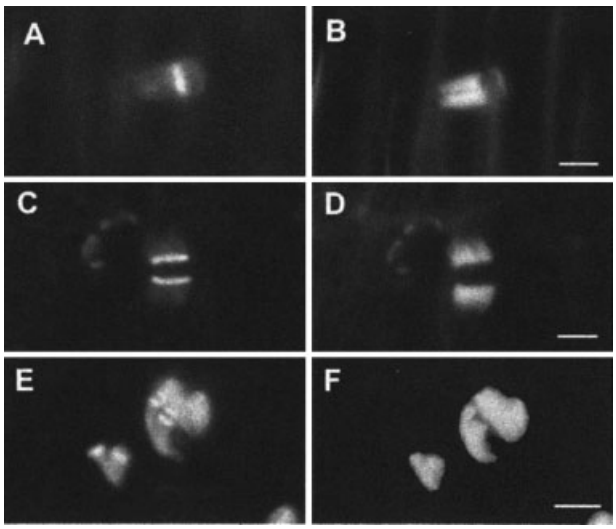

Fig. 2. Short-term (A–D) and long-term (E, F) incorporation of fluorescent actin beneath EPEC attached to pedestals. A,B: PtK2 cells infected with EPEC were permeabilized and exposed for 1 min to 0.3 μM rhodamine labeled monomeric actin. **A:** Rhodamine actin is concentrated just beneath the EPEC. **B:** The phalloidin counter-stain reveals the full extent of the pedestal actin beneath the attached EPEC. C,D: Similar short-term incorporation in a double pedestal. **C:** Note that actin is incorporated under each membrane-binding site along the two sides of an EPEC bacterium. **D:** Phalloidin staining reveals the total F-actin in the pedestals on either side of the EPEC. E,F: PtK2 cells infected with EPEC were permeabilized and exposed for 10 min to 0.3 μM rhodamine labeled monomeric actin. **E:** Rhodamine actin is incorporated all along the lengths of the single and double pedestals. Note the brighter area of rhodamine actin just beneath the attached bacteria. **F:** Phalloidin staining of the pedestals in E. Scale bar = μm.

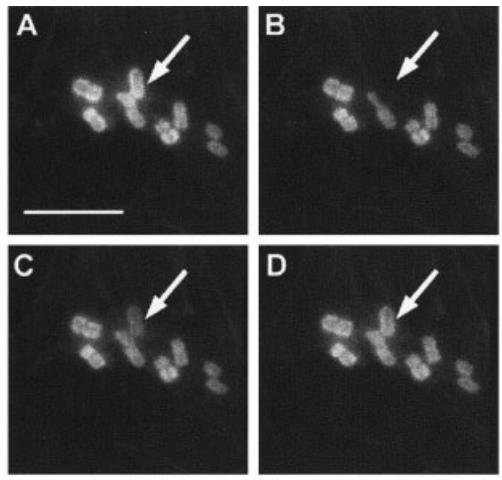

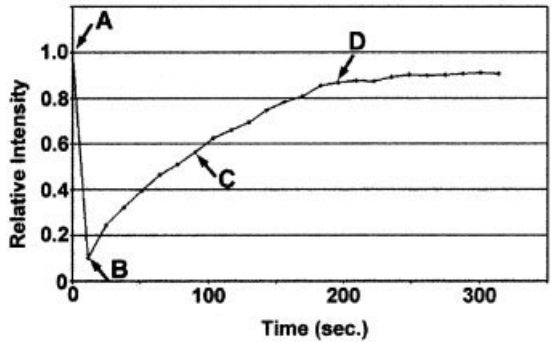

Fig. 3. Four time points (**A–D**) of a PtK2 cell transfected with GFP-actin and infected with EPEC. GFP-actin in a short pedestal beneath a single EPEC (*arrows*) was photobleached and recovery of fluorescence was recorded at the time points indicated on the graph. The *letters* on the graph correspond to the time when the images (A–D) were recorded. The half time of recovery was approximately 79 sec in this experiment. Scale bar = 10 μm.

length of single and double pedestals (Fig. 2E,F). There was no actin incorporation in the presence of 5 μM cytochalasin-D (data not shown).

Photobleaching of GFP-Actin in Short Pedestals

Fluorescence Recovery After Photobleaching or FRAP is a quantitative optical method that permits the detection of the exchange of fluorescently labeled molecules. To determine how dynamic the actin in bacteria-induced pedestals was, host cells were transfected with GFP- or YFP-actin and then infected with bacteria. In cells with short pedestals, less than 0.5 μm fluorescent actin was concentrated directly beneath the attached bacteria. The short EHEC pedestals were between 0.1 and 0.2 μm, while the short EPEC pedestals reached lengths up to 0.5 μmicrons. When the actin was photobleached, fluorescence intensity recovered with an average half time of 84 ± sec (n = 10) for EPEC (Fig. 3) and 74 ± 7 sec (n = 9) for EHEC. After approximately 5 min., the recovered intensity was close to or equal to the original intensity. The length of these pedestals was measured using z-sectioning of confocal microscopy, and the half-time for fluorescence recovery was assumed to be the time for half of the length of the bleached actin to be replaced by fluorescent monomer. These measurements indicated that the rate of addition of actin was approximately 0.015 μm/sec (n = 3) for EPEC. The lengths of the pedestals were too close to the limit of the light microscope to determine the rate of actin addition in these short pedestals.

Photobleaching of GFP-Actin in Long Pedestals-Site of Actin Polymerization

Photobleaching all the fluorescent actin in a pedestal allowed the initial site of actin monomer addition to be determined in live cells. Consistent with the results presented above for permeabilized EPEC-infected cells, GFP-actin monomers added first under the attached bacteria (Fig. 4). The band of newly assembled fluorescent

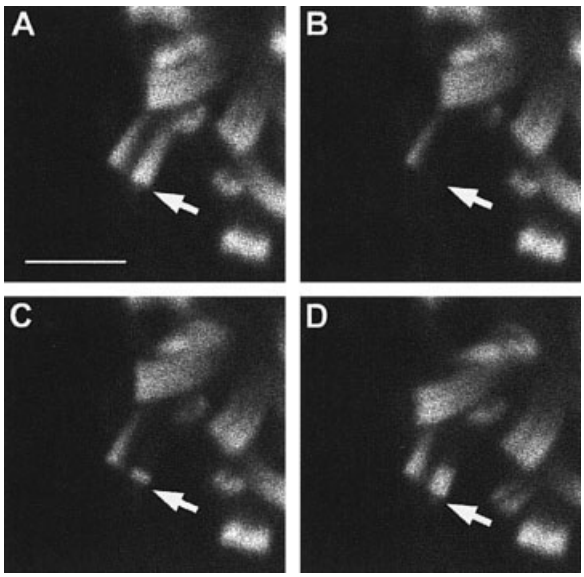

Fig. 4. PtK2 cells were transfected with YFP-actin and then infected with the JPN strain of EPEC. The entire long pedestal was photobleached, and actin fluorescence recovered starting at the tip of the pedestal (*arrows*) and moving at a constant rate towards the cell at 0.012 μm/second. **A:** Pre-bleach; **B:** bleach; **C:** 40 sec; **D:** 2 min. Scale bar = 10 μm.

actin increased in length at a constant rate. The speed of new actin length addition inferred from these observations is 0.016 ± 0.001 μm/sec (n = 40) for EPEC (Fig. 4) and 0.003 ± 0.001 μm/sec (n = 6) for EHEC (Fig. 5).

Stationary Pedestals Versus Translocating Pedestals

Sanger et al. [1996] demonstrated that EPEC pedestals had the potential of translocating along the surfaces of the infected host cells. When GFP-actin was bleached in pedestals of constant length that remained fixed in position on the cell membrane, the bleached band moved rearward down the pedestal as the pedestal remained stationary (Fig. 6A–E). In contrast, when a band was bleached in GFP-actin in pedestals of constant length that translocated along the cell surface, the location of the bleached band remained fixed with respect to the host cell and the band of newly assembled fluorescent actin grew beneath the attached bacterium as it moved forward (Fig. 6F–J). In stationary but elongating pedestals, the photobleached band also remained in a fixed position relative to the surface of the host cell (Fig. 7A–F). The rate of growth of the band of newly assembled fluorescent actin was approximately 1 μm/min (0.016 μm/sec) in both moving (Fig. 6F–J) and stationary pedestals (Figs. 6A–E, 7), and was unrelated to pedestal length.

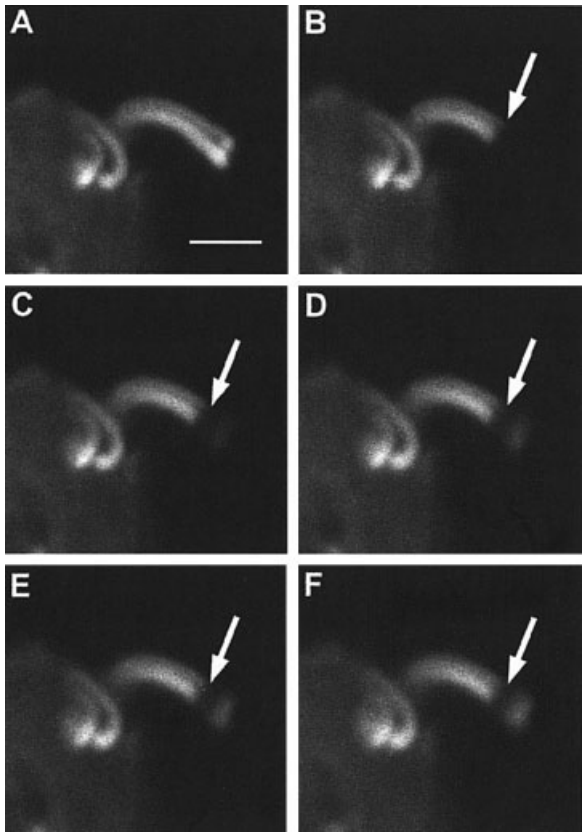

Fig. 5. GFP-actin transfected PtK2 cell infected with EHEC at the end of long immobile pedestals. A narrow band of GFP-actin was photobleached at the end of the pedestal beneath the EHEC. The bleached band (*arrows*) retained its shape and moved away from the bacterium at a slow rate of 0.48 μm/min. **A:** Pre-bleach; **B:** bleach; **C:** 39 s; **D:** 79 s; **E:** 118 s; **F:** 158 s. Scale bar = 5 μm.

Bleached Monomeric Actin Assembles in a Narrow Dark Band Before GFP-Actin Assembles

When a wide band was bleached from near the tip to the base in a long pedestal (Fig. 8), a narrow dark band often was observed within the newly assembled band of fluorescent actin shortly after the photobleach event (Fig. 8A–D). A kymograph illustrating the movement of the dark band with respect to time and position in the pedestal demonstrates that the band remains at the same position relative to the bleached band over time (Fig. 8, kymograph). This is presumably due to bleached GFP-actin monomers in the photobleached zone diffusing up to the tip of the pedestal and polymerizing before the pool of monomer GFP-actin from unbleached areas of the cell arrived at the tip. In stationary pedestals, the dark band moved back at same rate as the bleached band, the same rate as new actin length addition. In moving pedestals, the dark band remained fixed with respect to position on host cell (as in Fig. 8).

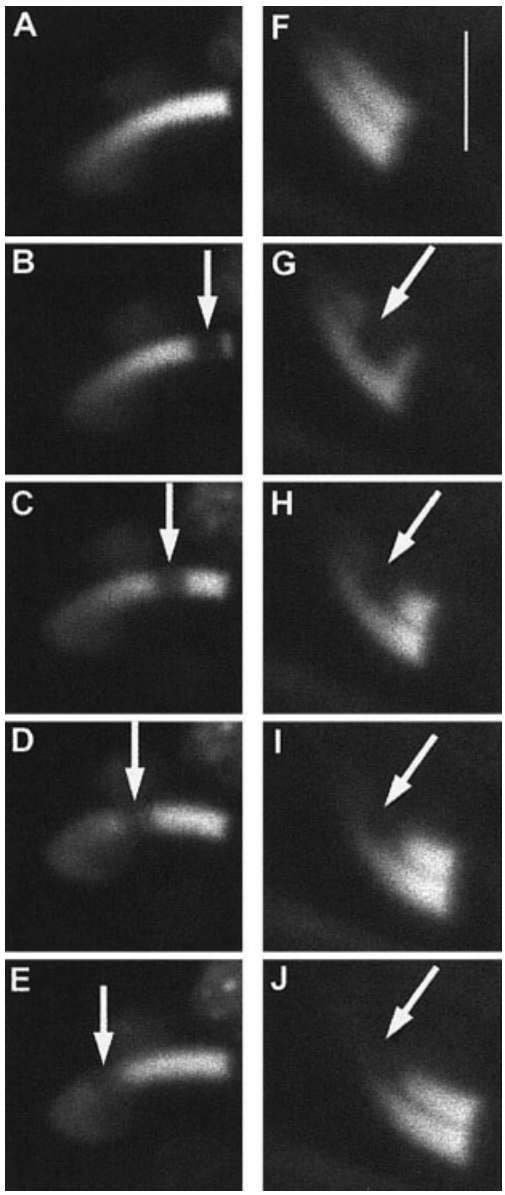

Fig. 6. Comparison of GFP-actin fluorescence recovery after photobleaching of a stationary long pedestal versus a translocating long pedestal. Narrow bands (*arrows*) were photobleached across each pedestal. The bleached band on the stationary pedestal moved away from the bacterium towards the cell body (**left**). The bleached band on the translocating pedestal remained stationary relative to the cell body, but moved distally with respect to the attached EPEC (**right**). **A:** Pre-bleach; **B:** bleach; **C:** 79 s; **D:** 145 s; **E:** 211 s; **F:** pre-bleach; **G:** bleach; **H:** 53 s; **I:** 106 s; **J:** 159 s. Scale bar = 5 μm.

Photobleaching of Fluorescent Alpha-Actinin in Pedestals

In contrast to the polarized recovery of GFP-actin fluorescence following photobleaching, the fluorescence of GFP- or YFP-alpha-actinin that was bleached in long pedestals recovered first in the area closest to the pedestal base and moved vertically upward toward the tip. Bands bleached in GFP-alpha-actinin expressing pedestals did not move down the pedestal, but rather remained stationary with their edges becoming blurred as they slowly regained fluorescence, presumably by diffusion of fluorescent alpha-actinin from the cell body into the pedestal (Fig. 9 A–D). In the long pedestals that were bleached, fluorescence intensity of GFP-alpha-actinin recovered to 54 ± 8% of the pre-bleach intensity level in a half-time of 61 ± 5 sec (n = 9). Whereas in short pedestals, the recovery of fluorescence was typically complete in 5 min with a half-time of recovery of 53 ± 13 sec (n = 10).

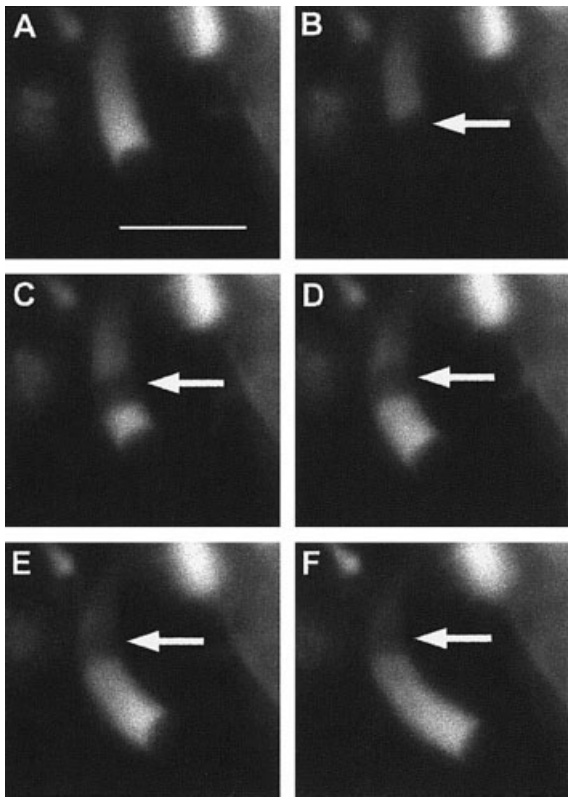

Fig. 7. GFP-actin transfected PtK2 cell infected with EPEC. Some pedestals were observed to elongate, with their bases remaining fixed with respect to the host cell, but the tip moving, i.e., length being added. The actin polymerization rate was same for these cases as in stationary and fixed-length moving cases. The bleached band (*arrows*) either remained stationary with respect to the host cell, as in this figure, or moved back towards host cell at a rate slower than the new actin length addition rate, resulting in net length addition to the pedestal. **A:** Pre-bleach; **B:** bleach; **C:** 66 s; **D:** 132 s; **E:** 198 s; **F:** 263 s. Scale bar = 5 μm.

Effect of BDM and Sodium Azide/2-Deoxy D-Glucose on Actin Dynamics in Pedestals

Different concentrations of BDM were used to test whether myosin might be involved in pedestal motility,

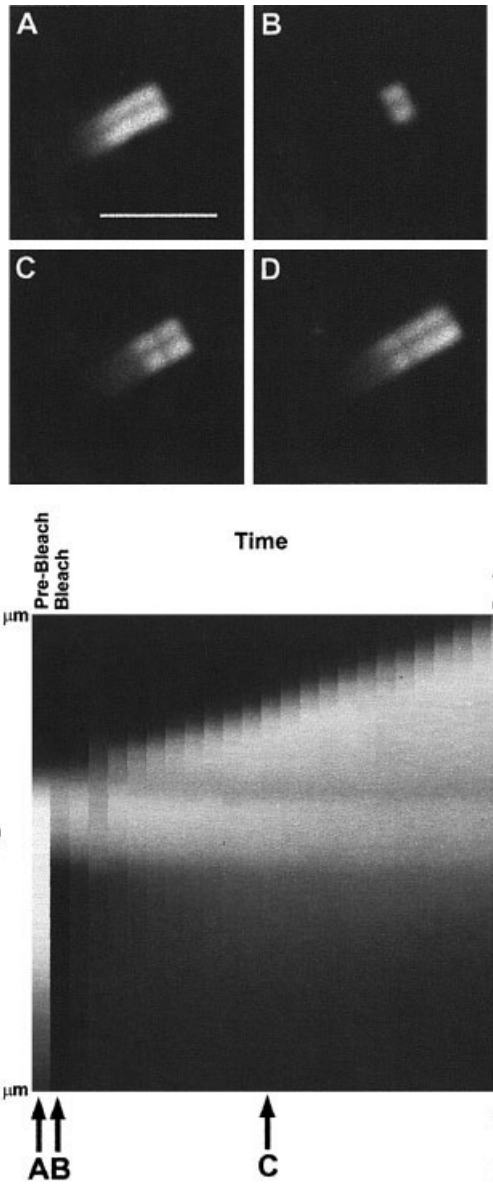

Fig. 8. GFP-actin transfected PtK2 cell infected with EPEC (**A–D**). A wide band was photobleached across a translocating pedestal (B). The bleached band remained stationary with respect to the host cell as actin polymerized beneath the attached EPEC (B to D). The kymograph shows all of the time points that were collected. A, B, C, and D (**bottom panel**) refer to the four time points in the images **A–D**. The horizontal axis represents time and the vertical axis represents position with respect to the substrate. Brightness corresponds to pedestal fluorescence. Note that the pedestal tip extends forward with time. Time point A shows the pre-bleach fluorescence profile and B indicates fluorescence that remains immediately after bleaching. The *dark line* runs horizontally across the kymograph indicating its fixed position relative to the substrate and to the original position of the pedestal tip (A). A: pre-bleach; B: bleach; C: 130 s; D: 5 min. Scale bar = 10 μm.

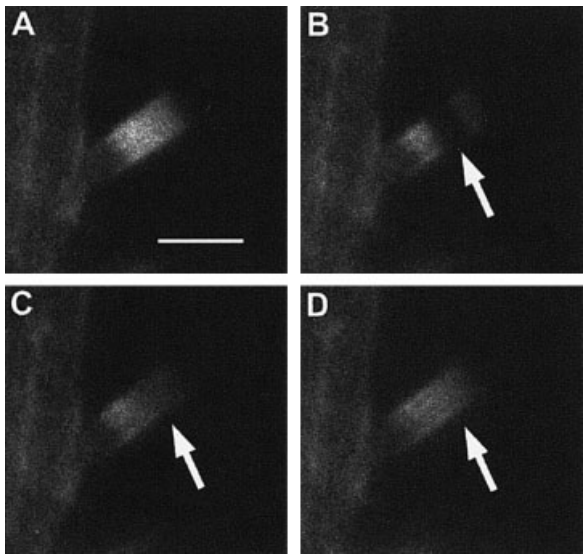

Fig. 9. YFP-alpha-actinin transfected PtK2 cell infected with EPEC (**A**). A band of YFP-alpha-actinin (*arrow* in **B**) was photobleached beneath one EPEC. Fluorescence recovery was observed at indicated time points (**C,D**). The half time of recovery for this example was approximately 46 sec. Alpha-actinin fluorescence recovers first at the base of the bleached spot and moves up the pedestal towards the externally attached bacterium. This pattern differs from recovery of actin fluorescence where the initial recovery is always at the membrane beneath the externally attached EPEC (compare with Fig. 4). The GFP-alpha-actinin intensity in long pedestals never recovers to the pre-bleach intensity. Furthermore, there is no sign of a photobleached band moving down the pedestal as is observed in photobleached pedestals containing fluorescently labeled actin (compare with Fig. 6). A: Pre-bleach; B: bleach; C: 39 s; D: 105 s. Scale bar = 5 μm.

on the initial assumption that BDM was an inhibitor of non-muscle myosin II [Cramer and Mitchison, 1995, 1997; Lin et al., 1996]. We exposed EPEC-infected PtK2 cells, transfected with GFP-actin, to BDM at concentrations ranging from 10 to 50 mM. At all concentrations, BDM induced pedestals to grow unusually long, producing lengths up to 50 μm (Fig. 10A,B). Removal of the inhibitor resulted in reduced pedestal lengths within minutes. Cycles of pedestal elongation or shortening were freely reversible. When GFP-actin in pedestals was photobleached in the presence of BDM, the bleached bands remained fixed in place, and newly assembled fluorescent actin was added at the tip (Fig. 10C–F) in the absence of depolymerization along the pedestal or at its base (Fig. 10B). As a result, the pedestals grew very long. Removal of BDM led to the transformation of the long pedestals to shorter ones, with retrograde flow of the labeled actin towards the center of the cell. Subsequent to these experiments, Ostap [2002] demonstrated that although BDM did inhibit skeletal muscle myosin II, the drug did not inhibit the ATPase activity of several different non-muscle myosins from the classes I, II, V, and VI. We also tested the effect of

ML-7, an inhibitor of the light chain kinase of non-muscle myosin II, that causes filament disassembly of non-muscle myosin II [Burridge, and Chrzanowska-Wodnicka, 1996; Du et al., 2003], and observed no effects on the rearward movement of actin or on the translocation of pedestals in infected cells previously transfected with GFP-actin (data not shown).

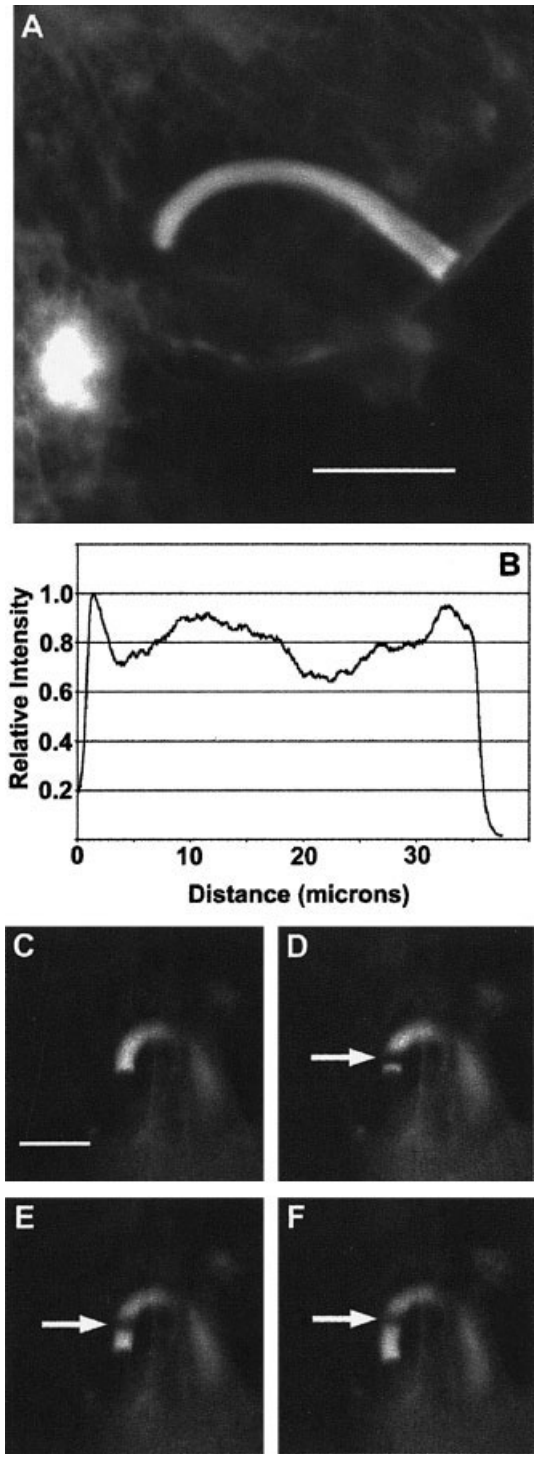

When the ATP concentration in cultures of EPEC/EHEC-infected cells was reduced with the combination of sodium azide (20 mM) and 2-deoxy D-glucose (10 mM), the effect on pedestal movement and the depolymerization of actin in the pedestals was similar to the effect of BDM, leading to similarly long pedestals (Fig. 11). As in BDM-treated cells, pedestals in EPEC-infected cells were longer than those in EHEC-infected cells, reaching lengths of up to 20 μm (Fig. 11). Similarly, removal of sodium azide and 2-deoxy D-glucose led to shortening of the pedestals, and the resumption of the rearward flow of the tagged actin filaments inside the shorter pedestals. Cycles of lengthening and shortening could be repeated several times with addition and removal of the inhibitors.

Photobleaching of fluorescent actin in pedestals in the presence of the ATP inhibitors displayed a biphasic response that depended on the time of exposure to the inhibitors. Overall, in the first 10 to 20 min in the presence of the inhibitors, actin added to the area underneath the externally attached bacteria, but actin filaments did not move or depolymerize. After 30 min of exposure to the ATP inhibitory drugs, there was no addition of fluorescent actin to the area beneath the bacteria and there was no loss of actin in the pedestals. However, once the drugs were washed out, the pedestals responded to photobleaching as described for normal pedestals.

Effect of BDM and Sodium Azide/2-Deoxy D-Glucose on Active and Inactive Forms of Cofilin

Cofilin, known to sever actin filaments, is present in the pedestals of EPEC- and EHEC-infected cells [Goosney et al., 2001] and might, therefore, promote the actin depolymerization seen in pedestals. In its phosphorylated form, cofilin is inactive in promoting actin depolymerization [Meberg et al., 1998]. To examine cofilin phosphorylation with respect to conditions inhibiting pedestal actin depolymerization (BDM and sodium azide/2-deoxy D-glucose), uninfected cultures of PtK2 cells were treated with 50 mM BDM, or 20 mM sodium azide and 10 mM 2-deoxy D-glucose. As controls, cul-

Fig. 10. PtK2 cells were infected with JPN strain EPEC and treated with 50 mM BDM for 30 min. Pedestals became unusually long, with many exceeding 25 to 30 μm in length. **A:** BDM-induced 30-μm-long pedestal (stained with Alexa488-Phalloidin). **B:** Fluorescence intensity scan along BDM-induced pedestal (see A), indicating F-actin concentration. There is a brighter region at the tip of the pedestal followed by a very broad plateau. **C–F:** A band of photobleached YFP-actin failed to move back along the pedestal while the tip continued to grow at 0.017 μm/sec, the same rate as for non-BDM-treated pedestals. The pedestal in C–F grows from to 10 to 16 μm during this exposure to BDM. C: Pre-bleach; D: 0 min; E: 2 min; F: 4 min. Scale bar = 10 μm.

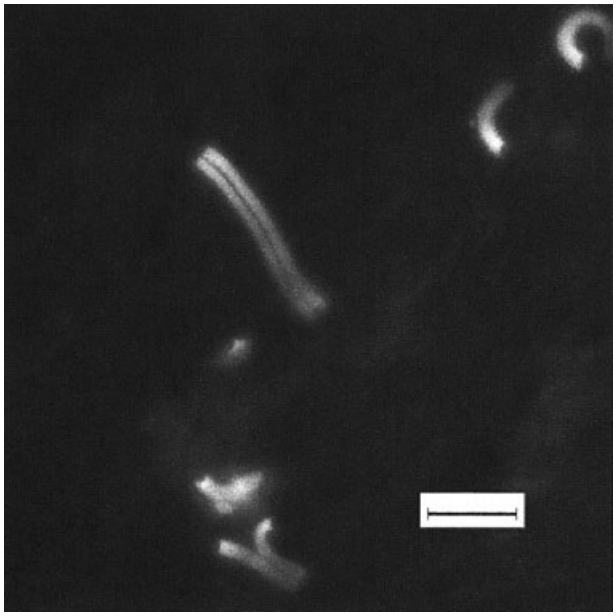

Fig. 11. PtK2 cells infected with EPEC were exposed to sodium azide/2-deoxyglucose for 30 min before fixation and staining with fluorescent phalloidin. The pedestals grow to long lengths in these treated cells, reaching lengths of up to 50 μm. Scale bar = 10 μm.

tures were untreated or treated with 10 nM PMA (phorbal 12-myristate 13-acetate), an activator of protein kinase C. Western analysis of cell lysates was performed using specific antibodies directed against phosphorylated cofilin (inactive cofilin) and dephosphorylated cofilin (active cofilin) (Fig. 12). In cells treated with 20 mM sodium azide and 10 mM 2-deoxy D-glucose, phosphorylated cofilin (inactive form) was depleted (as might have been expected). BDM had no detectable effect on the phosphorylation state of cofilin. Thus, although both BDM and 20 mM sodium azide and 10 mM 2-deoxy D-glucose treatments inhibit actin depolymerization in pedestals, neither treatment caused a decrease in the active, dephosphorylated cofilin. These experiments suggest that the inhibitors may be blocking the depolymerization action of active cofilin (unphosphorylated) by a pathway that does include the inactivation or phosphorylation of cofilin.

DISCUSSION

The adhesion of EHEC/EPEC bacteria to host cells produces specialized attachment plaques beneath the bacteria on the dorsal surface of the infected cells [Goosney et al., 2000b; Huang et al., 2002]. Actin filaments that assemble at these sites form bundles that evaginate to form membrane-covered projections termed pedestals [Knutton et al., 1987, 1989; Kaper et al., 2004]. EPEC/EHEC pedestals range from 0.25 to 10 μm long, and can undergo both elongation and shortening. The longer pedestals can undulate and translocate on the cell surfaces of infected cells [Sanger et al., 1996]. The ability of EPEC to form pedestals has been correlated with the extent of the diarrhea that was induced in human volunteers [Donnenberg et al., 1993]. The pedestals may provide an advantageous environment for EHEC/EPEC growth and residence inside animals, by allowing the bacteria to remain attached to intestinal cells during (1) peristalsis and (2) the host flushing response to rid itself of infectious bacteria [Hecht, 1999]. An alternative view is that pedestals are an advantage for the host when infected cells with pedestal-attached bacteria undergo apoptosis causing the removal of the infected cells with their attached bacteria from the body [Malish et al., 2003]. In a recent report by Deng et al. [2003] on intestinal infections by Citrobacter rodentium of live mice, results were presented that questioned whether actin pedestal formation is required for efficient colonization and disease. These authors speculated that the C. rodentium Tir inserted into the mouse intestinal cells could achieve localization by direct binding of either alpha-actinin [Freeman et al., 2000] or integrin [Frankel et al., 1996].

The site of initial addition of actin monomers to the ends of the actin filaments just beneath the membrane attachment sites in saponized infected cells (Fig. 2) mirrored the initial site of fluorescence recovery in bleached pedestals in infected cells that had been transfected with GFP-actin (Fig. 4). Longer incubations with monomer actin and longer times of recovery of fluorescence of GFP-actin after bleaching eventually resulted in fluorescent actin incorporation along the entire length of the pedestals. This is consistent with a model proposed for the coupling of intracellular actin polymerization at the barbed ends of actin filaments to the formation of pedestals [Sanger et al., 1996]. The mode suggests that the barbed ends available for polymerization are present exclusively at the proximal ends of the pedestals. This could occur if the actin filaments were continuous in length from tip to base in the pedestals, or if capping proteins bound the barbed ends of shorter actin filaments in the pedestals. The findings presented here suggest there is a decreasing concentration of actin filaments from tip to base (Fig. 1), perhaps resulting from depolymerization of some actin filaments occurring along the length of the pedestal.

When the EPEC-encoded protein, Tir, is inserted in a host cell membrane, its middle or extracellular domain binds the bacterial membrane protein, intimin. The third Tir domain (intracellular carboxyl terminal domain) of EPEC, but not of EHEC, contains a tyrosine that is phosphorylated by host cell proteins [DeVinney

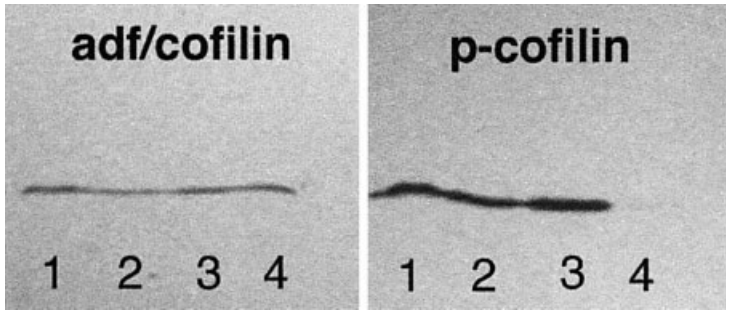

Fig. 12. Specific antibodies directed against activated cofilin (adf/cofilin) and the inactivated or phosphorylated cofilin (p-cofilin) were used to determine if BDM or sodium/azide decreased the levels of active cofilin. Western blots showing phosphorylated (p-cofilin) and unphosphorylated cofilin (adf/cofilin) in extracted PtK2 cells. **Lane 1:** Control cells; **lane 2:** cells treated with 10 nM PMA (phorbal 12-myristate 13-acetate, an activator of protein kinase C); **lane 3:** cells treated with 50 mM BDM; **lane 4:** cells treated with 20 mM sodium azide and 10 mM 2-deoxy D-glucose. There was no depletion of the active form of cofilin (lanes 3 and 4 in adf/cofilin Western blot), although both BDM and sodium azide/2-deoxy D-gluclose inhibited actin depolymerization in the pedestals. Treatment of PtK2 cells with sodium azide/2-deoxy D-glucose depleted the inactive form of cofilin (lane 4 in p-cofilin blot).

et al., 1999; Kenny, 1999; Goosney et al., 2000b]. This tyrosine phosphorylation of the third domain of Tir permits the recruitment of Nck, Grb2, and CrkII to the EPEC pedestals [Goosney et al., 2001; Gruenheid et al., 2001; Campellone et al., 2002]. This Nck binding recruits N-WASP and the Arp2/3 complex to the tip of the pedestal, initiating actin polymerization [Gruenheid et al., 2001]. Campellone et al. [2004] have reported that the removal of the first cytoplasmic domain of EPEC Tir is not necessary for actin polymerization and pedestal formation. A similar removal of the first cytoplasmic domain for EHEC was not attempted. Although the Tir receptor of EHEC does not bind the adapter protein Nck [Gruenheid et al., 2001], EHEC is still capable of assembling actin pedestals. In Nck-null cells, EHEC, but not EPEC, is able to induce the formation of pedestals [Gruenheid et al., 2001]. Whereas there was no difference in actin dynamics between the two closely related strains of EPEC (E2348/69 and JPN-15), there was a striking difference in actin dynamics in long pedestals between EPEC and EHEC. Long pedestals of EHEC-infected cells (Fig. 5) showed a fivefold slower rate of actin polymerization than occurred in EPEC long pedestals. It was difficult to compare the rates of actin polymerization in short pedestals because EHEC short pedestals are typically less than 0.25 μm, compared with 0.5 to 2 μm for EPEC (Fig. 3). Our FRAP results are consistent with the idea that Nck binding to Tir accelerates actin polymerization more efficiently than the mechanism employed by EHEC Tir.

Pedestals could be grouped into four types within the 5–10 min they were subjected to FRAP analysis: (1) constant length and stationary; (2) increasing in length and stationary; (3) constant length and translocating; (4) increasing in length and translocating. A surprising finding of the FRAP analysis was that in all pedestals, regardless of length or position (Fig. 6A), actin polymerization occurred at the pedestal tip at an average rate of 1 μm per second. We were unable to determine the initial rate of actin polymerization in brand new pedestals. There is the possibility that this rate might be different from that measured in existing pedestals. Only in stationary pedestals of constant length, did retrograde flow of actin occur (Fig. 6A–E). Furthermore, the bleached band always retained its shape with no compression as it moved rearward. In a pedestal where most of the actin was bleached (Fig. 8), the thin band of non-fluorescent actin that first assembled at the pedestal tip remained stationary with respect to the host cell as fluorescent actin was then added to the tip at a rate of approximately 1 μm/min. In uninfected PtK2 cells, bands bleached in GFP-actin in lamellipodia also moved rearward at nearly the same rate (data not shown).

The elongated geometry of the pedestals and their isolation from the cell body permitted us to photobleach both the pool of monomeric actin as well as F-actin. This allowed us to detect the polymerization of bleached monomers as a dark line between two fluorescent bands, the fluorescent band present behind the tip at the time of bleaching and the fluorescent band that formed after bleaching. This dark line is a demonstration that photobleached monomers are not prevented from polymerizing at the tip of the pedestal. For the example in Figure 8, the width of the dark band was measured to be approximately 0.35 μm. Since the rate of length addition due to actin polymerization was measured to be 0.013 μm/sec for this pedestal, this width corresponds to a time of approximately 27 sec. Taking this as the time for fluorescent actin monomers to diffuse up the length of the pedestal, a distance of 6.4 μm, we calculated the diffusion coefficient for GFP-actin in this pedestal to be 2.5×10^{-9} cm^2/sec.

Previous studies [McGrath et al., 1998] have measured actin diffusion coefficients in bovine aortic endothelial cells to be 3.1×10^{-8} cm^2/sec. The tenfold difference in measured values can be attributed to the larger size of GFP-tagged actin, and to the different environment inside the EPEC pedestal compared to the cytoplasm.

The retrograde movement of actin filaments in the pedestals is reminiscent of the rearward flow of fluorescently labeled actin from the edges of stationary cells (0.8 μm/min) detected with FRAP analysis [Wang, 1985]. However, the composition and structure of pedestals appear to be very different from that of lamellipodia. The cellular micro-composition of pedestals can be thought of as a cross between lamellipodia, microvilli, and focal adhesions. Like microvilli, pedestals have villin and ERM proteins distributed along their lengths with tropomyosin and non-muscle myosin II at the base of the pedestals [Goosney et al., 2001; Sanger et al., 1996]. Photobleaching of GFP-actin in the focal adhesions of these PtK2 cells did not reveal any flow of actin molecules there (data not shown). Like focal adhesions, pedestals have alpha-actinin, talin, and vinculin localized along their length [Freeman et al., 2000; Goosney et al., 2001]. Similar photobleaching of focal adhesions containing GFP-alpha-actinin revealed a replacement of the photobleached alpha-actinin with new GFP-alpha-actinin but no flow of alpha-actinin along the length of the attachments [Dabiri et al., 1999; Edlund et al., 2001]. The presence of Arp2/3 in the EPEC/EHEC pedestals suggests that the actin filaments should be branched as they are in lamellipodia. This is consistent with transmission electron micrographs that do not reveal any signs of long parallel actin filaments in pedestals [Knutton et al., 1987; Kaper et al., 2004]. Steady state fluorescence polarization methods that predicted aligned filaments around the periphery of *Listeria* actin tails [Zhukarev et al., 1995] failed to detect aligned actin filaments in EPEC pedestals (Zhukarev et al., unpublished observations).

Bleached bands of GFP-alpha-actinin in pedestals (Fig. 9) recovered fluorescence in a completely different manner from photobleached bands of GFP-actin. The bleached band did not move down the pedestal, and when the whole pedestal was photobleached, fluorescent alpha-actinin could be seen to diffuse in from the unbleached part of the cell producing fluorescence recovery from the base toward the tip. Recovery of the intensity of GFP-alpha-actinin fluorescence occurred only to about half of the pre-bleach intensity level in long pedestals, but in short pedestals, recovery was typically complete in 5 min. This difference may be a function of the distance required for diffusion of protein into short pedestals as compared to that distance for long pedestals. We interpret these results to indicate that alpha-actinin exchanges constantly all along the pedestal at a rate much faster than actin polymerization so that the pattern of alpha-actinin does not follow the actin movement.

The translocation of EPEC pedestals is known to require actin polymerization [Sanger et al., 1996], and as predicted [Sanger and Sanger, 1992], the rate of movement was coupled to the rate of actin polymerization at the pedestal tip (Figs. 6F–J, 7). What was unexpected was that the rate of actin polymerization in both moving and stationary pedestals would be the same. As discussed in the model below, the interplay of actin polymerization and depolymerization could alone provide the physical parameters leading to pedestal movement, recognizing in the cellular environment that there are many proteins that modulate actin-based motility and may influence pedestal motility.

BDM (2,3-butanedione monoxime) has been used as an inhibitor of actin/myosin interactions in cross-striated and smooth muscles due to its inhibitory effect on cross-bridge attachment, phosphorylation of smooth muscle myosin light chains, and the movement of actin filaments along myosin II [Adams et al., 1998; Siegman et al., 1994]. It also affects intracellular calcium mobilization in living muscle cells [Siegman et al., 1994]; however, in skinned muscle fibers, where there is no calcium uptake and release, BDM also inhibits force production [McKillop et al., 1994]. We used BDM because of the *initial* idea that BDM also affected the activity of non-muscle myosin II [Cramer and Mitchison, 1995, 1997; Lin et al., 1996]. The reversible inhibition by BDM of actin depolymerization and the retrograde flow of actin filaments in pedestals (Fig. 10) initially suggested that a myosin motor might be involved in this process. However, ML-7, an inhibitor of non-muscle myosin II, had no effect on the flow of actin in pedestals. It is now known that BDM affects the ATPase activity of muscle myosin IIs but not non-muscle myosin II or the unconventional myosins [Ostap, 2002]. Nevertheless BDM affected the depolymerization and rearward movement of the actin filaments in pedestals. BDM (1 to 50 mM) has been reported to reversibly inhibit retrograde flow and stimulate extension of neuronal growth cones [Lin et al., 1996]. Interpreted at the time in terms of a role for non-muscle myosin, it may be that BDM may be exerting these effects in neuronal cells by interfering with actin depolymerization as it does in EPEC pedestals. We have tested (1) BDM and (2) sodium azide/2-deoxy-glucose, on Listeria-infected PtK2 cells, and discovered a similar reversible inhibition of actin depolymerization in actin tails leading to elongation of the tails up to 50 μm [Shaner et al., 2002]. These experiments further support the idea that these inhibitors are exerting their effects on EPEC/EHEC pedestals by interfering with the depolymerization of F-actin.

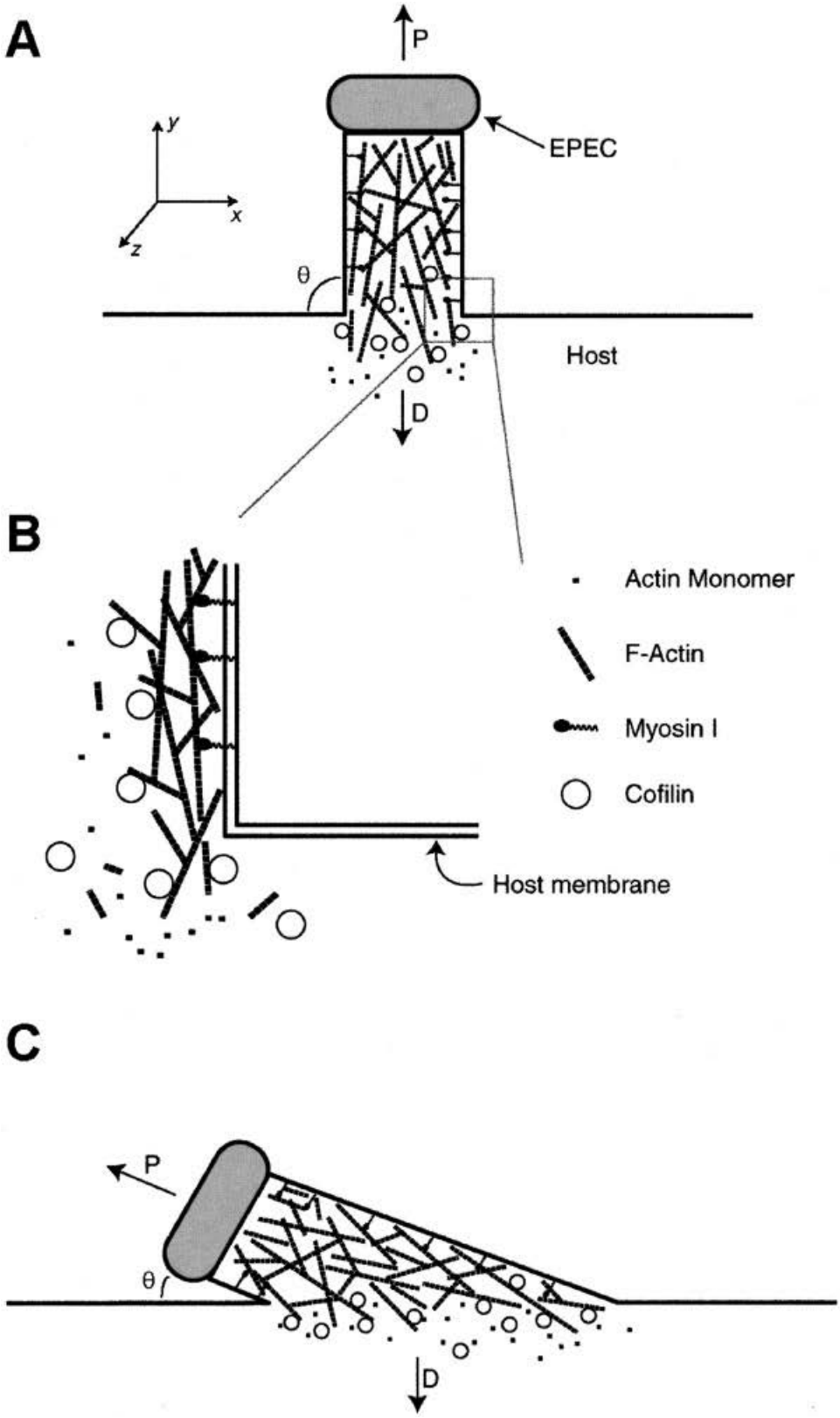
A
P
EPEC
y
x
z
θ
Host
D
B
Actin Monomer
F-Actin
Myosin I
Cofilin
Host membrane
C
P
θ
D

Figure 13.

Since cofilin is thought to play an important role in the depolymerization of actin filaments in cells [Meberg et al., 1998], the inhibitors BDM or sodium azide/2-deoxy D-glucose that stabilized the actin filaments in the pedestals might have been expected to cause a depletion of the active or dephosphorylated form of cofilin. This did not occur. When cells are treated with sodium azide and 2-deoxy D-glucose, there is an inferred buildup of inorganic phosphate since intracellular levels of ATP drop from 2 to 4 mM to 100 μM in 30 min [Glascott et al., 1987]. Stapleton et al. [1998] have reported that BDM accelerates the loss of ATP in cells treated with sodium azide and 2-deoxy-glucose. It is not known if BDM treatment alone would also lead to decreases in intracellular ATP. Millimolar levels of inorganic phosphate (Pi) are known to inhibit cofilin-mediated actin depolymerization in a test tube [Blanchoin et al., 2000]. Thus, an increase in intracellular Pi would protect F-actin from the action of active cofilin. Future experiments will be needed to test this suggestion. Our experiments do demonstrate that actin continues to polymerize at the pedestal tip, but this length addition to the pedestal is no longer balanced by depolymerization at the base, and so a dramatic increase in pedestal length occurs.

Although the mechanisms by which BDM and sodium azide/2-deoxy D-glucose affect actin depolymerization and retrograde flow in the pedestals is unknown, these results do indicate that actin depolymerization is required for the rearward flow of actin and the translocation of the pedestals along the cell surface. How actin polymerization and depolymerization may generate translocations of pedestals is discussed in the model section below (Fig. 13).

MODEL FOR THE TRANSLOCATION OF PEDESTALS

The EPEC pedestal can be modeled as a column (or probably a hollow tube) of cross-linked, branched actin filaments whose mostly capped plus ends are oriented towards the tip of the pedestal. Arp2/3 nucleated actin polymerization is highly localized and directional, and occurs at the tip of the pedestal directly beneath the attached bacterium. Arps are all along the pedestals [Goosney et al., 2001]. Yet pulse incorporation and FRAP indicates actin monomers adding just beneath the EPEC attachment site. The host cell membrane is stabilized along the actin column by myosin I and presumably other proteins that link cortical actin to the membrane, e.g., alpha-actinin and villin [Sanger et al., 1996; Freeman et al., 2000; Shaner et al., 2002]. Actin filaments exposed to the cytoplasm in the center of the pedestal are gradually depolymerized, primarily by cofilin, which is known to be localized all along the pedestal [Kalman et al., 1999]. However, the majority of the actin filaments in the pedestal appear to be somewhat protected from depolymerization (Fig. 1), possibly by their association with the membrane and their tight bundling, until the point at which the pedestal joins the host cell and the minus ends of the actin filaments are exposed on all sides to the host cell cytoplasm (Fig. 13B). At this point, cofilin-mediated depolymerization destroys most of the remaining filaments within a short time.

For photobleaching analysis, we chose pedestals that were in a single focal plane along most or all of their length. EPEC pedestals that were stationary with respect to the host cell extended from the edge of the cell, at an angle close to 90° with the host cell membrane (Fig. 13A). In contrast, translocating pedestals were always observed to be on the surface of the host cell. For our observations, those pedestals confined to a single focal plane on the surface of the host cell had to be at a small angle with the host cell membrane. For a pedestal at an angle to the host cell membrane, F-actin was observed to move only in a direction perpendicular to the host cell membrane, and never laterally along the host cell.

Translocation of pedestals is observed only for pedestals that are at a very steep angle with the host cell membrane. That is, the interface between the host cell and the pedestal is nearly parallel with the long axis of the pedestal. In this case, the myosin I-mediated stabilization of the pedestal occurs primarily on the dorsal side of the pedestal, with the ventral side being mostly exposed to the host cell cytoplasm, and so easily depolymerized by the action of cofilin. With this geometry, also, membrane elasticity should tend to push the F-actin in the pedestal down towards the host cell mostly in a direction normal to the surrounding host cell membrane. While actin polymerization continues to occur parallel to the long axis of the pedestal, depolymerization now occurs mostly perpendicular to the host cell membrane. Because length addition to the pedestal tip and length

Fig. 13. In an EPEC pedestal, actin polymerization occurs directly beneath the attached bacterium, while depolymerization important in motility occurs at the interface between the pedestal and the host cell cytoplasm (**A**). In the proposed model for EPEC pedestal motility, the pedestal is composed of a network of actin filaments cross-linked by alpha-actinin and other proteins. When actin filament ends enter the cytoplasm at the base of the pedestal, actin monomers are released from the filament and it shortens by some number of monomers (**B**). Over time, this leads to the uniform slipping of the entire pedestal toward the host cell body. When the pedestal is at an angle smaller than 90° with the host cell membrane (**C**), the interface between the pedestal and the host cell cytoplasm remains parallel to the host cell membrane, and so the pedestal base processes sideways as actin monomers are removed.

subtraction from its base occur independently and with different directionality, the vector difference between the polymerization and depolymerization gives rise to the translocation of the pedestal along the host cell surface. This can be simply described mathematically in terms of the vectors of actin polymerization and depolymerization.

Actin monomers that are incorporated into the pedestal tip are drawn from the soluble pool of actin in the host cell cytoplasm, which diffuses quickly throughout the cell, as revealed by whole-pedestal and half-cell photobleaching experiments. As actin monomers are added to the tip of the pedestal, the host cell membrane is pushed out through a Brownian ratchet mechanism. The rate of length addition to the pedestal due to the actin polymerization-driven Brownian ratchet at the tip can be described as:

$$\check{p} = \alpha P[\cos\theta\hat{i} + \sin\theta\hat{j}],$$

where P is the rate of polymerization of actin in monomers added per second, θ is the angle the pedestal makes with the host cell membrane (Fig. 13C), and α is the length per actin monomer. Unit vectors in the x- and y-directions are $\hat{i}$ and $\hat{j}$, respectively.

If D is the depolymerization rate at the pointed ends of actin filaments at the pedestal base, then the rate of length subtraction from the pedestal due to actin depolymerization by cofilin can be described as:

$$\check{d} = -|\alpha D|\hat{j}.$$

Since the vast majority of pedestals are observed to be of constant length, it is likely that an equilibrium between polymerization and depolymerization is reached relatively quickly. This suggests that in most cases, $|D| = |P\sin\theta|$. When this is the case, and $\theta < 90^\circ$, the net effect of combined polymerization at the tip and depolymerization at the base is the movement of the pedestal base and the pedestal tip an equal distance in the x-direction, parallel to the host cell membrane. For arbitrary P and D, pedestal elongation should occur if $|D| < |P\sin\theta|$, and pedestal shortening (observed very infrequently) should occur if $|D| > |P\sin\theta|$.

In general, if we know the initial position, $\check{r}_0$, of an attached EPEC at the tip of a pedestal, its position over time based on length addition and removal rates due to actin polymerization and depolymerization is given by:

$$\check{r}(t) = \left[\check{p} + \check{d}\right]t + \check{r}_0$$
$$\check{r}(t) = \alpha[P\cos\theta\hat{i} + (P\sin\theta - D)\hat{j}]t + \check{r}_0.$$

Pedestals at an angle $<90^\circ$ to the host cell membrane will, therefore, translocate along the surface of the host cell (Fig. 13C).

ACKNOWLEDGMENTS

This work was supported by grants from the United States Department of Agriculture (Research Institute Competitive Grants Program of the USDA) to J.M.S. The authors are indebted to Dr. Nancy Freeman for her insightful comments on the manuscript and to Dr. Andrea Stout for her cogent criticisms of our modeling section.

REFERENCES

Adams W, Trafford AW, Eisner DA. 1998. 2, 3-Butanedione monoxime (BDM) decreases sarcoplasmic reticulum Ca content by stimulating Ca release in isolated rat ventricular myocytes. Pflugers Arch Eur J Physiol 436:776–781.

Ayoob JC, Sanger JM, Sanger JW. 2000a. Visualization of the expression of Green Fluorescent Protein (GFP) linked genes. In: Tuan RS, Lo CW, editors. Methods in molecular biology: developmental biology protocols, Vol. III. Totowa, NJ: Humana Press. p 153–157.

Ayoob JC, Turnacioglu KK, Mittal B, Sanger JM, Sanger JW. 2000b. Targeting of cardiac titin fragments to Z-bands and dense bodies of living muscle and non-muscle cells. Cell Motil Cytoskeleton 45:67–82.

Ayoob JC, Shaner NC, Sanger JW, Sanger JM. 2001. Expression of Green or Red Fluorescent Protein (GFP or DsRed) linked proteins in non-muscle and muscle cells. Mol Biotechnol 17:65–71.

Batchelor M, Guignot J, Patel A, Cummings N, Cleary J, Knutton S, Holden DW, Connerton I, Frankel G. 2004. Involvement of the intermediate filament protein cytokeratin-18 in actin pedestal formation during EPEC infection. EMBO Rep 5:104–110.

Blanchoin L, Pollard TD, Mullins RD. 2000. Interactions of ADF/cofilin, Arp2/3 complex, capping protein and profilin in remodeling of branched actin filament networks. Curr Biol 10:1273–1282.

Burridge K, Chrzanowska-Wodnicka M. 1996. Focal adhesions, contractility and signaling. Ann Rev Cell Dev Biol 12:463–519.

Campellone KG, Griese A, Tipper DJ, Leong JM. 2002. A tyrosine-phosphorylated 12-amono acid sequence of enteropathogenic *Escherichia coli* Tir binds the host adaptor protein Nck and is required for Nck localization to actin pedestals. Mol Microbiol 43:1227–1241.

Campellone KG, Rankin S, Pawson T, Kirschner MW, Tipper DJ, Leong JM. 2004. Clustering by Nck by a 12-residue Tir phosphopeptide to trigger localized actin assembly. J Cell Biol 164:407–416.

Cantarelli VV, Takahashi A, Yanagihara I, Akeda Y, Imura K, Kodama T, Kono G, Sato Y, Iida T, Honda T. 2002. Cortactin is necessary for F-actin accumulation in pedestal structures induced by enteropathogenic *Escherichia coli* infection. Infect Immun 70:2206–2209.

Carlier MF, Nioche P, Broutin-L'Hermite I, Boujemaa R, Le Clainche C, Egile C, Garbay C, Ducruix A, Sansonetti P, Pantaloni D. 2000. GRB2 links signaling to actin assembly by enhancing interaction of neural Wiskott-Aldrich syndrome protein (ARP2/3) complex. J Biol Chem 275:21946–21952.

Cossart P, Sansonetti PJ. 2004. Bacterial invasion: the paradigms of enteroinvasive pathogens. Science 304:242–248.

Cramer L, Mitchison TJ. 1995. Myosin is involved in post-mitotic cell spreading. J Cell Biol 131:179–189.

Cramer L, Mitchison TJ. 1997. Investigation of the mechanism of retraction of the cell margin and rearward flow of nodules during mitotic cell rounding. Mol Biol Cell 8:109–119.

Cudmore SP, Reckmann I, Griffiths G, Way M. 1996. Vaccinia virus; a model system for actin-membrane interactions. J Cell Sci 109:1739–1747.

Dabiri G, Sanger JM, Portnoy DA, Southwick FS. 1990. *Listeria monocytogenes* moves rapidly through the host cell cytoplasm by inducing directional actin assembly. Proc Natl Acad Sci USA 87:6068–6072.

Dabiri G, Turnacioglu KK, Sanger JM, Sanger JW. 1997. Myofibrillogenesis visualized in living embryonic cardiomyocytes. Proc Natl Acad Sci USA 94:9493–9498.

Dabiri G, Ayoob JC, Turnacioglu KK, Sanger JM, Sanger JW. 1999. Use of Green Fluorescent Proteins linked to cytoskeletal proteins to analyze myofibrillogenesis in living cells. Methods Enzymol 302:171–186.

Deng W, Vallance BA, Li Y, Puente JL, Finlay BB. 2003. Citrobacter rodentium translocated intimin receptor (Tir) is an essential virulence factor needed for actin condensation, intestinal colonization and colonic hyperplasia in mice. Mol Microbiol 48:95–115.

DeVinney R, Stein M, Reinscheid D, Abe A, Ruschkowski S, Finlay BB. 2001a. Enterohaemorrhagic *Escherichia coli* O157:H7 produces Tir, which is not tyrosine phosphorylated. Infect Immun 67:2389–2398.

DeVinney R, Puente JL, Gauthier A, Goosney D, Finlay BB. 2001b. Enterohaemorrhagic and enteropathogenic *Escherichia coli* use a different Tir-based mechanism for pedestal formation. Mol Micro 41:1445–1458.

DeVinney R, Stein M, Reinscheid D, Abe A, Ruschkowski S, Finlay BB. 1999. Enterohemorrhagic *Escherichia coli*: 015:H7 produces Tir, which is translocated to the host cell membrane but is not tyrosine phosphorylated. Infect Immun 67:2389–2398.

Donnenberg MS, Tacket CO, James SP, Losonsky G, Nataro JP, Wasserman SS, Kaper JB, Levine MM. 1993. Role of the eaeA gene in experimental enteropathogenic *Escherichia coli* infection. J Clin Infect 92:1412–1417.

Du A, Sanger JM, Linask KK, Sanger JW. 2003. Myofibrillogenesis in the first cardiomyocytes formed from isolated quail precardiac mesoderm. Dev Biol 57:382–394.

Edlund MM, Lotano A, Otey CA. 2001. Dynamics of alpha-actinin in focal adhesions and stress fibers visualized with alpha-actinin-Green Fluorescent Protein. Cell Motil Cytoskeleton 48:190–200.

Frankel G, Lider O, Hershkoviz R, Mouth AP, Kachalsky SG, Dandy D, Cahalon L, Humphries MJ, Dougan G. 1996. The cell binding domain of intimin from enteropathogenic *Escherichia coli* binds to beta1 integrins. J Biol Chem 271:20359–20364.

Freeman NL, Zurawski DV, Chowrashi P, Ayoob JC, Huang L, Mittal B, Sanger JM, Sanger JW. 2000. Interaction of the enteropathogenic *Escherichia coli* protein, tralocated intimin receptor (Tir), with focal adhesion proteins. Cell Motil Cytoskeleton 47:307–318.

Frischnecht F, Way M. 2001. Surfing pathogens and the lessons learned for actin polymerization. Trends Cell Biol 11:30–38.

Glascott PA, McSorley K, Mittal B, Sanger JM, Sanger JW. 1987. Stress fiber reformation after ATP depletion. Cell Motil Cytoskeleton 8:118–129.

Goosney DL, Devinney R, Pfuetzner RA, Frey EA, Strynadka NC, Finlay BB. 2000a. Enteropathogenic *Escherichia coli* translocated intimin receptor interacts directly with alpha-actinin. Curr Biol 10:735–738.

Goosney DL, Gruenheid S, Finlay BB. 2000b. Gut feelings: enteropathogenic *Escherichia coli* (EPEC) interactions with the host. Annu Rev Cell Dev Biol 16:173–189.

Goosney DL, Devinney R, Finlay BB. 2001. Recruitment of cytoskeletal and signaling proteins to Enteropathogenic and Enterohemorrhagic *Escherichia coli* pedestals. Infect Immun 69:3315–3322.

Gruenheid S, DeVinney R, Bladt F, Goosney D, Gelkop S, Gish GD, Pawson T, Finlay BB. 2001. Enteropathogenic *E. coli* Tir binds Nck to initiate actin pedestal formation in host cells. Nature Cell Biol 3:856–859.

Hecht G. 1999. Innate mechanisms of epithelial host defense: spotlight on intestine. Am J Physiol 277:C351–C358.

Huang L, Mittal B, Sanger JW, Sanger JM. 2002. Host focal adhesion protein domains that bind to the translocated intimin receptor (Tir) of Enteropathogenic *Escherichia coli* (EPEC). Cell Motil Cytoskeleton 52:255–265.

Ismali A, Philpott DJ, Dytoc MT, Soni R, Ratnam S, Sherman PM. 1995. Alpha-actinin accumulation in epithelial cells infected with attaching and effacing gastrointestinal pathogens. J Infect Dis 172:1393–1396.

Jerse AE, Yu J, Tall BD, Kaper JB. 1990. A genetic locus of enteropathogenic *E. coli* necessary for the production of attaching and effacing lesions on tissue culture cells. Proc Natl Acad Sci USA 87:7839–7843.

Kalman D, Weiner OD, Goosney DL, Sedat JW, Finlay BB, Abo A, Bishop JM. 1999. Enteropathogenic *E. coli* acts through WASP and Arp2/3 complex to form actin pedestals. Nature Cell Biol 1:389–391.

Kaper JB, Nataro JP, Mobley LT. 2004. Pathogenic *Escherichia coli*. Nature Rev Micro 2:123–140.

Kenny B. 1999. Phosphorylation of tyrosine 474 of the enteropathogenic *Escherichia coli* (EPEC) Tir receptor is essential for actin nucleation. Mol Microbiol 31:1229–1241.

Kenny B, DeVinney R, Stein M, Reinscheid DJ, Frey EA, Finlay BB. 1997. Enteropathogenic *E. coli* (EPEC) transfers its receptor for intimate adherence into mammalian cells. Cell 91:511–520.

Knutton S, Baldini MM, Williams PH, McNeish AS. 1989. Role of plasmid-encoded adherence factors in adhesion of enteropathogenic *Escherichia coli* to HEp-2 cells. Infect Immun 55:78–85.

Knutton S, Lloyd DR, McNeish AS. 1987. Adhesion of Enteropathogenic *Escherichia coli* to human intestinal enterocytes and cultured human intestinal mucosa. Infect Immunol 55:69–77.

Lin CH, Espreaficio EM, Mooseker MS, Forscher P. 1996. Myosin drives retrograde F-actin flow in neuronal growth cones. Neuron 16:769–782.

Lommel S, Benesch S, Rottner K, Franz T, Wehland J, Kuehn R. 2001. Actin pedestal formation by enteropathogenic *Escherichia coli* and intracellular motility of Shigella flexneri are abolished in N-WASP-defective cells. EMBO Rep 21:850–857.

Lommel S, Benesch S, Rohde M, Wehland J, Rottner K. 2004. Enterohaemorrhagic and enteropathogenic *Escherichia coli* use different mechanisms for actin pedestal formation that converge on N-WASP. Cell Microbiol 6:243–254.

Malish HR, Freeman NL, Zurawski DV, Chowrashi P, Ayoob JC, Sanger JW, Sanger JM. 2003. Potential role of the EPEC translocated intimin receptor (Tir) in host apoptotic events. Apoptosis 8:179–190.

McGrath JL, Tardy Y, Dewey CF Jr, Meister JJ, Hartwig JH. 1998. Simultaneous measurements of actin filament turnover, filament fraction, and monomer diffusion in endothelial cells. Biophys J 75:2070–2078.

McKillop DFA, Fortune NS, Ranatunga KW, Geeves MA. 1994. The influence of 2, 3-butane 2-monoxime (BDM) on the interaction between actin and myosin in solution and in skinned muscle fibres. J Mus Res Cell Motil 15:309–318.

Meberg PJ, Ono S, Minamide LS, Takahashi M, Bamburg JR. 1998. Actin depolymerizing factor and cofilin phosphorylation dynamics: response to signals that regulate neurite extension. Cell Motil Cytoskeleton 39:172–190.

Ostap EM. 2002. 2, 3-butanedione monoxime (BDM) as a myosin inhibitor. J. Mus Res Cell Motil 23:305–308.

Rosenshine I, Ruschkowski S, Stein M, Reinscheid DJ, Mills SD, Finlay BB. 1996. A pathogenic bacterium triggers epithelial signals to form a functional bacterial receptor that mediates actin pseudopod formation. EMBO J 15:2613–2624.

Sanger JM, Sanger JW, Southwick FS. 1992. Host cell actin assembly is necessary and likely to provide the propulsive force for the intracellular movement of *Listeria monocytogenes*. Infect Immun 60:3609–3619.

Sanger JM, Chang R, Ashton F, Kaper JB, Sanger JW. 1996. Novel form of actin-based motility transports bacteria on the surfaces of infected cells. Cell Motil. Cytoskeleton 34:279–287.

Sanger JW, Sanger JW. 1992. Beads, bacteria and actin. Nature 357:442.

Sanger JW, Sanger JM, Jockusch BM. 1983. Differential response of three types of actin filament bundles to depletion of cellular ATP levels. Eur J Cell Biol 31:197–204.

Shaner NC, Sanger JW, Sanger JM. 2002. Lowering of cellular ATP levels inhibits actin depolymerization in EPEC/EHEC pedestals and *Listeria* tails. Mol Biol Cell 13:177a.

Siegman MJ, Mooers SU, Warren TB, Warshaw DM, Ikebe M, Butler TM. 1994. Comparison of the effects of 2, 3-butanedione monoxime on force production, myosin light chain phosphorylation and chemical energy usage in intact and permeabilized smooth and skeletal muscle. J Mus Res Cell Motil 15:457–472.

Stapleton MT, Fuchsbauer CM, Allshire AP. 1998. BDM drives protein dephosphorylation and inhibits adenine nucleotide exchange in cardiomyocytes. Am J Physiol 275:H1260-6.

Symons M, Mitchison TJ. 1991. Control of actin polymerization in live and permeabilized cells. J Cell Biol 114:503–513.

Turnacioglu KK, Sanger JW, Sanger JM. 1998. Sites of monomeric actin incorporation in living PtK2 and REF-52 cells. Cell Motil Cytoskeleton 40:59–70.

Wang Y-L. 1985. Exchange of actin subunits at the leading edge of living fibroblasts: possible role of treadmilling. J Cell Biol 101:597–602.

Zhukarev V, Ashton FT, Sanger JM, Sanger JW, Shuman H. 1995. Steady state fluorescence polarization study of actin filament bundles in *Listeria*-infected cells. Cell Motil. Cytoskeleton 30:229–246.